

Interatomic Coulombic electron capture in H^+-Li and H^+-He-Li systems: The role of He as an intermediate species

Ju Meng(孟举), Zhitao Pang(庞志涛), Kedong Wang(王克栋)

Citation: Chin. Phys. B. 35, 093401 (2026). DOI: 10.1088/1674-1056/ae37fe |
CSTR: 32038.14.CPB.ae37fe
http://cpb.iphy.ac.cn; http://iopscience.iop.org/cpb

What follows is a list of articles you may be interested in

Spin- and state-resolved charge transfer and excitation in low-energy He+–Na(3s,3p) collisions

Xiao-Xia Wang(王小霞), Rui Tang(唐瑞), Li Ma(马丽), Chuan-Yu Zhang(张传瑜), Jian-Guo Wang(王建国), Yi-Zhi Qu(屈一至)
Chin. Phys. B. 35, 073402 (2026). DOI: 10.1088/1674-1056/ae705c | CSTR: 32038.14.CPB.ae705c

Charge transfer processes in low-energy Na+–Na collisions

Cheng-Cheng Jiang(蒋承呈), Xiao-Xia Wang(王小霞), Kun Wang(王堃), Yi-Zhi Qu(屈一至), Jian-Guo Wang(王建国), Xia Li(李侠), Li Ma(马丽), Robert J. Buenker
Chin. Phys. B. 35, 043402 (2026). DOI: 10.1088/1674-1056/ae15f0 | CSTR: 32038.14.CPB.ae15f0

Single electron capture in low- and intermediate-energy collisions of Si3,4+ with He

Yingzhou Li(李英卓), Yadong Liu(刘亚东), Yueying Qi(祁月盈), Ling Liu(刘玲), Yizhi Qu(屈一至), Jianguo Wang(王建国)
Chin. Phys. B. 35, 013401 (2026). DOI: 10.1088/1674-1056/ae15f4 | CSTR: 32038.14.CPB.ae15f4

State-selective single- and double-electron capture in collisions of low-energy S5+ ions with helium

Yixin Fan(樊依鑫), Dadi Xing(邢大地), Shucheng Cui(崔述成), Xiaoxia Wang(王小霞), Junxia Ran(冉俊霞), Kaizhao Lin(林楷钊), Xubin Zhu(朱旭斌), Dongmei Zhao(赵冬梅), Dalong Guo(郭大龙), Yong Gao(高永), Shaofeng Zhang(张少锋), Xiaolong Zhu(朱小龙), Xinwen Ma(马新文)
Chin. Phys. B. 34, 073402 (2025). DOI: 10.1088/1674-1056/adcb9a | CSTR: 32038.14.CPB.adcb9a

Fragmentation dynamics of nitric oxide induced by low-energy heavy ions

Zhixin Li(李志欣), Kaizhao Lin(林楷钊), Xiaolong Zhu(朱小龙), Zhiliang Li(李志亮), Hang Yuan(苑航), Yong Gao(高永), Dalong Guo(郭大龙), Dongmei Zhao(赵冬梅), Shaofeng Zhang(张少锋), Xinwen Ma(马新文)
Chin. Phys. B. 34, 053401 (2025). DOI: 10.1088/1674-1056/adbdc0 | CSTR: 32038.14.CPB.adbdc0

Interatomic Coulombic electron capture in H^+–Li and H^+–He–Li systems: The role of He as an intermediate species

Ju Meng(孟举), Zhitao Pang(庞志涛), and Kedong Wang(王克栋)†

School of Physics, Henan Normal University, Xinxiang 453007, *China*

(Received 23 December 2025; revised manuscript received 10 January 2026; accepted manuscript online 14 January 2026)

Interatomic Coulombic electron capture (ICEC) is an environment-assisted electron capture mechanism where a free electron efficiently attaches to a quantum system by transferring its excess energy to a neighboring atom or molecule, thereby ionizing it. In this study, we explore electron attachment in the H^+–Li and H^+–He–Li systems, emphasizing the role of the intermediate He species in the ICEC process. The calculations are performed using the *ab initio R*-matrix method, combined with the configuration interaction method to account for electronic correlation. Convergence is tested by varying active spaces and the number of partial waves in the Legendre expansion for the one-electron and two-electron integrals. When the ICEC process involves He^- as a virtual intermediate state, our results show that He can significantly enhance ICEC efficiency. In contrast, when He acts merely as a geometric intermediate without participating as a virtual state, its presence has little effect on the direct ICEC process between H^+ and Li. Pronounced resonance features are observed in the ICEC cross sections, and the partial contributions are analyzed in detail.

Keywords: electron capture, *ab initio R*-matrix method

PACS: 34.80.Bm

DOI: 10.1088/1674-1056/ae37fe **CSTR:** 32038.14.CPB.ae37fe

1. Introduction

Interatomic Coulombic electron capture (ICEC) is a process in which a free electron is efficiently captured by an acceptor A (i.e., atom, molecule, quantum dot), while its excess energy is non-radiatively transferred to a neighboring electron-donor system B, resulting in the ionization of B. It was shown that the environment can strongly enhance the electron capture cross sections by atoms and ions compared to the capture by the isolated species A. ICEC might thus be a general process underlying the damage of living cells under ionizing radiation as well as a major actor in the electron-mediated chemistry that leads to the formation of pre-biotic species in interstellar environments.[1]

ICEC was first predicted in 2009 by Gokhberg and Cederbaum,[2,3] who concluded that ICEC can dominate over photorecombination (PR) even at ion-neighbor distances of a few nanometers. Remme *et al.*[4] showed that the presence of an additional third atom can greatly enhance this interatomic process when the capture transition energy in the first atom resonates with a dipole-allowed excitation in the assisting atom — a mechanism known as three-center resonant electron capture. In contrast to these calculations based on analytical models, Sisourat and coworkers[5] used an *ab initio R*-matrix method to compute the ICEC cross sections. They found that their calculated cross sections were much larger than those predicted by the asymptotic formula, primarily due to orbital overlap. Subsequently, using the same method, they investigated electron attachment to a proton in water. They[6,7] investigated the Fano interferences and how the distortion of the equilibrium geometry of the water molecule influences the ICEC process. Later, they[8] reported the contribution of virtual photon exchange and electron transfer to the total ICEC cross section as a function of the distance between the charged and neutral particles. With a different method, based on the multiconfiguration time-dependent Hartree (MCTDH) approach and complex absorbing potential, Sisourat and coworkers[9] performed time-dependent quantum simulations and studied the impact of the nuclear motion on ICEC.

ICEC is closely related to the interparticle Coulombic decay (ICD) process. Although both share the same fundamental decay mechanism, they differ in their initiation: ICEC is triggered by electron capture, whereas ICD begins with the creation of an inner-shell vacancy. Recently, Miteva *et al.*[10] showed that a helium atom can function as a bridge in the Ne^+–Ne system, significantly enhancing the efficiency of ICD, due to the resonance state of $Ne^+He^-Ne^+$. Bennett *et al.*[11] investigated three-body ICD within the virtual photon approximation, incorporating macroscopic quantum electrodynamics, and demonstrated that the presence of a passive atom can significantly modify the ICD rate. Similarly, Kuleff[12,13] studied related processes by examining electronic decay in OC_nF_2 and $HOCnH(2n-1)F_3$ using the multielectron wavepacket propagation method. Their results showed

†Corresponding author. E-mail: wangkd@htu.edu.cn

© 2026 Chinese Physical Society and IOP Publishing Ltd. All rights, including for text and data mining, AI training, and similar technologies, are reserved.

that the decay proceeds more efficiently along the carbon chain than through free space. Despite these advances, the influence of the surrounding medium on ICEC decay processes has not yet been explored.

The objective of this work is to investigate the role of helium as an intermediate species in the ICEC process involving a proton and a lithium atom. Using the *ab initio* *R*-matrix method,[14] we compute both total and partial ICEC cross sections for the H^+–Li and H^+–He–Li systems. To ensure the reliability of the results, various computational models were tested to verify the convergence of the cross sections. Furthermore, this study explores resonance structures in the ICEC cross sections, providing a theoretical basis to support potential experimental observations of the process.

2. Computational details

The ICEC process can be viewed as a scattering interaction between the captured electrons and the system. The *R*-matrix method has been extensively used in the study of low-energy electron scattering with multi-atomic molecules, making it suitable for analyzing the ICEC process.[5,15–17] In the fixed-nuclei (FN) approximation, the *R*-matrix approach divides the coordinate space into an inner and an outer region, with the coordinate system's origin placed at the molecule's center of mass. The inner region includes the N electrons of the molecule and one continuum electron, and the identical nature of these electrons leads to significant electron correlation and exchange effects. In the inner region, the wave function is written using the form of a close-coupling (CC) expansion

$$\Psi_k(\boldsymbol{x}_1\cdots\boldsymbol{x}_{N+1}) = \mathcal{A}\sum_{ij}\alpha_{ijk}\phi_i(\boldsymbol{x}_1\cdots\boldsymbol{x}_N)u_{ij}(\boldsymbol{x}_{N+1}) + \sum_i \beta_{ik}\chi_i(\boldsymbol{x}_1\cdots\boldsymbol{x}_{N+1}), \quad (1)$$

where $\mathcal{A}$ is an antisymmetrization operator, ϕ_i is the multiparticle wavefunction of the N-electron target state i, u_{ij} represents the spin-coupled continuum orbitals, here, representing the incident and outgoing electrons in ICEC. The second term represents the short-range correlation and polarization effects, χ_i are the L^2 configurations that can be generated by setting all $N+1$ electrons in target molecular orbitals. To obtain the coefficients α_{ijk} and β_{ik}, the matrix obtained from the sum of the $(N+1)$ Hamiltonian and the Bloch operator[18] is diagonalized. The inner region must be large enough to completely contain the N-electron wave function of the target. In the outer region, the effects of electron correlation are considered negligible, and the scattering electron is treated as interacting solely with the multipolar potential field of the target molecule. The *R*-matrix method facilitates the matching of wavefunctions at the boundary between the two regions, with the *R*-matrix being computed using the energy-independent wavefunction in the inner region, $\Psi(\boldsymbol{x}_1\cdots\boldsymbol{x}_{N+1})$, as given in Eq. (1). By propagating the *R*-matrix to larger distances and matching it to the asymptotic solutions, the *K*-matrix is obtained. The eigenphase sums, cross section (via the *S* matrix), and other scattering data can be obtained from the *K*-matrix.

In our calculations, the H^+–He–Li is assumed to have a linear structure. The structure of H^+–He–Li is shown in Fig. 1. The distances between H^+ and He, He and Li, and H^+ and Li are denoted as R_1, R_2, and R, respectively. In *R*-matrix electron-molecule scattering calculations, the symmetry is reduced from $C_{\infty v}$ to C_{2v} due to computational limitations. Finite point groups like C_{2v} are compatible with standard codes and basis sets and allow efficient, symmetry-consistent treatment of the system. Wavefunctions were obtained using the restricted Hartree–Fock (RHF) method implemented in the MOLPRO package.[19] The RHF electronic configuration for the ground state of H^+–He–Li is $1\sigma^2 2\sigma^2 3\sigma^1$, while that for H^+–Li is $1\sigma^2 2\sigma^1$. To describe the target states, we use the complete active space configuration interaction (CAS-CI) method, implemented in the UKRmol+ package[20,21] with 6-311G(2df,2pd) basis sets. For H^+–He–Li, three different active spaces are explored: CAS(5,10), consisting of orbitals 1–$6a_1$, 1–$2b_1$, and 1–$2b_2$, CAS(5,11), with orbitals 1–$7a_1$, 1–$2b_1$, and 1–$2b_2$, CAS(5,14), including orbitals up to $8a_1$, $3b_1$, and $3b_2$. In all cases, no core electrons are frozen, and all five electrons are allowed to occupy the designated active orbitals freely.

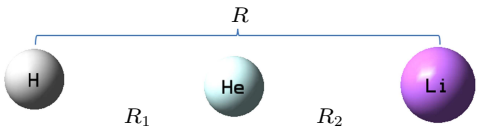


Fig. 1. The structure for H^+–He–Li.

Table 1 lists the vertical excitation energies of the target states for the H^+–He–Li system, calculated at the CAS(5,11) level. The first seven states include the six lowest-energy states associated with the presence of a neutral lithium atom, as well as one state corresponding to the Li^+ cation, which represents the final state in the ICEC process. The first vertical excitation energy is 8.26 eV, representing the energy difference between the initial and final states involved in ICEC. This value is in good agreement with the known energy difference of 8.22 eV between the ground states of isolated hydrogen and lithium atoms.[22] The energy difference between the first and second excited states is 1.84 eV, corresponding to the first excitation energy of the Li atom. This value is also in excellent agreement with the experimental result of 1.85 eV reported in the Computational Chemistry Comparison and Benchmark Database (CCCBDB).[22] These results confirm the reliability and accuracy of our present calculations.

Table 1. Vertical excitation energies (T_v in eV) for the target states of H^+–He–Li and H^+–Li with $R_1 = R_2 = 8$ Å, $R = 16$ Å. The absolute ground-state energy for H(1s)–He–$Li^+(2s^{-1})$ and H(1s)–$Li^+(2s^{-1})$ is −10.5957 a.u. and −7.7357 a.u., respectively. The initial ICEC state is underlined, the final ICEC states are in regular font, and the lowest excited electronic states involving neutral Li are in bold.

Sym.	T_v for H^+HeLi	States for H^+HeLi	T_v for H^+Li	States for H^+Li
$^2A_1/^2\Sigma^+$	0.00	H(1s)-He–$Li^+(2s^{-1})$	0.00	H(1s)-$Li^+(2s^{-1})$
$\underline{^2A_1/^2\Sigma^+}$	$\underline{8.26}$	$\underline{H^+–He–Li(\tilde{X})(1^2\Sigma^+)}$	$\underline{8.26}$	$\underline{H^+–Li(\tilde{X})(1^2\Sigma^+)}$
$^2A_1/^2\mathbf{\Sigma^+}$	**10.10**	$\mathbf{H^+–He–Li^*}(2^2\Sigma^+)$	**10.10**	$\mathbf{H^+–Li^*}(2^2\Sigma^+)$
$^2B_1 + ^2B_2/^2\mathbf{\Pi}$	**10.11**	$\mathbf{H^+–He–Li^*}(1^2\Pi)$	**10.11**	$\mathbf{H^+–Li^*}(1^2\Pi)$
$^2A_1/^2\mathbf{\Sigma^+}$	**12.31**	$\mathbf{H^+–He–Li^*}(3^2\Sigma^+)$	**12.31**	$\mathbf{H^+–Li^*}(3^2\Sigma^+)$
$^2A_1/^2\mathbf{\Sigma^+}$	**12.82**	$\mathbf{H^+–He–Li^*}(4^2\Sigma^+)$	**12.82**	$\mathbf{H^+–Li^*}(4^2\Sigma^+)$
$^2B_1 + ^2B_2/^2\mathbf{\Pi}$	**12.83**	$\mathbf{H^+–He–Li^*}(2^2\Pi)$	**12.83**	$\mathbf{H^+–Li^*}(2^2\Pi)$
$^2B_1 + ^2B_2/^2\Pi$	21.49		63.67	
$^2B_1 + ^2B_2/^2\Pi$	24.25		68.47	
$^2A_2/^2\Sigma^-$	34.84		71.67	
$^2A_2/^2\Sigma^-$	35.27		72.24	
$^2A_2/^2\Sigma^-$	36.85		75.52	
$^2A_2/^2\Sigma^-$	37.04		75.83	
$^2A_2/^2\Sigma^-$	37.86		75.93	

The active space CAS(5,11) for H^+–He–Li includes the following orbitals: $1s_H$, $1s_{He}$, $1s_{Li}$, $2p_{Li}$. For consistency and ease of comparison, the corresponding orbitals of hydrogen and lithium are also included in the active space for the H^+–Li system. In the absence of the helium atom, the active space for H^+–Li is defined as 1–6a_1, 1–2b_1, and 1–2b_2. Using this active space and the 6-311G(2df,2pd) basis set, the vertical excitation energies for H^+–Li are also calculated and presented in Table 1. The results reveal that the H^+–Li system exhibits almost the same electronic structure characteristics as the H^+–He–Li system. As discussed above, these results show excellent agreement with available reference data, further validating the reliability of our computational approach.

In the present work, B-spline type orbitals (BTOs) are used to represent the continuum. Compared to Gaussian-type continuum orbitals, BTOs are easier to extend to higher angular momentum partial waves and offer better numerical stability. Continuum orbitals with angular momentum up to $\ell = 6$ are employed. The orthogonalization deletion threshold for BTOs is set to 10^{-6}. B-splines of order 6 are used, with a total of 30 radial B-splines included in the basis set. The first two radial B-splines are excluded because they possess a nonzero first derivative at the origin, which would violate smoothness conditions. In both the H^+–He–Li trimer and the H^+–Li dimer, the lighter proton is positioned farther from the center of mass compared to the other atoms. To ensure that the R-matrix sphere contains the N-electron wave function of the target, an R-matrix radius of $r = 30a_0$ is used for H^+–He–Li and $r = 36a_0$ for H^+–Li.

For the scattering calculations, the L^2 configurations are categorized into two classes: $(CAS)^5(virtual)^1$ and $(CAS)^6$. The R-matrix is propagated from the inner region boundary at r out to $100a_0$, ensuring that the continuum electron's radial wave function is converged to the asymptotic form at the propagation limit.

Convergence tests with respect to both the R-matrix radius and the propagation distance confirm the adequacy of this approach. A total of 18 target states, obtained from CAS-CI calculations, are included in the close-coupling expansion. Both singlet and triplet spin states are taken into account during electron capture processes. The expansion of the long-range multipole potential is truncated at the quadrupole term, retaining multipoles up to rank 2.

3. Test of models

We focus on the direct ICEC process, where one electron is captured by the proton to form the ground state of hydrogen, while the other electron is emitted from the ground state of lithium.

The total ICEC cross section results for H^+–He–Li with two different basis sets and three active spaces are presented in Fig. 2. As seen from the figure, the cross section results obtained using the 6-311G(d) and 6-311G(2df,2pd) basis sets exhibit nearly identical amplitudes within the same active space for both CAS(5,10) and CAS(5,11). This indicates that the 6-311G(2df,2pd) basis set is sufficiently flexible to yield converged results for the H^+–He–Li system under the present computational conditions.

Using this basis set, we observe that extending the active space from CAS(5,10) to CAS(5,11) — by including one additional virtual orbital — leads to an increase in the total cross section amplitude in the low-energy region (electron energies below 8.9 eV). To further verify convergence, we also tested a larger active space, CAS(5,14), with the same basis set. The results, also shown in Fig. 2, reveal a strong similarity between the CAS(5,11) and CAS(5,14) curves. This similarity suggests that polarization and correlation effects in the electron scattering process with H^+–He–Li are well accounted for in the CAS(5,11) model. In summary, the combination of the 6-311G(2df,2pd) basis set with the CAS(5,11) active space

provides an optimal balance between computational efficiency and accuracy. This setup is adopted for all subsequent calculations and analyses involving the H^+–He–Li system.

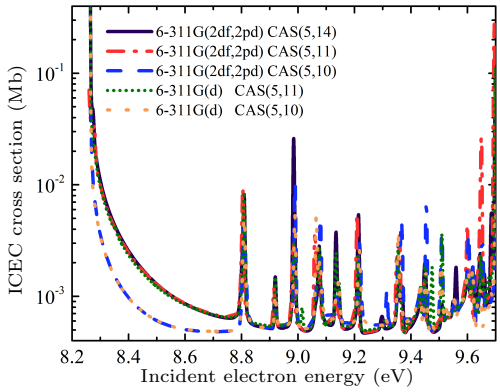


Fig. 2. ICEC cross section for H^+–He–Li obtained by summing the cross sections for singlet and triplet states with two different basis sets and three different active spaces for $R_1 = R_2 = 8$ Å.

The parameters single-electron-nucleus and two-electron integrals control the highest partial wave included in the Legendre expansion of the Coulomb potential when calculating the BTO integrals. In this work, we assess the influence of different truncation limits in the Legendre expansions of these integrals. Figures 3 and 4 present convergence tests for the H^+–Li and H^+–He–Li systems, respectively, using six different maximum angular momentum values in the Legendre expansions of the mixed nuclear attraction and two-electron integrals. As the maximum Legendre order increases, the computed cross sections for both systems gradually decrease, indicating improved accuracy. Convergence is nearly reached at an expansion limit of 70 and is clearly achieved at 80. For comparison, a previous study[8] employed maximum Legendre orders of 85 and 35 for the one-electron and two-electron integrals, respectively. We tested this combination and found that it yields results identical to those obtained with both limits set to 80. Considering the reduced computational cost, we adopt 85 and 35 as the respective maximum Legendre orders for the one-electron and two-electron integrals in all subsequent calculations.

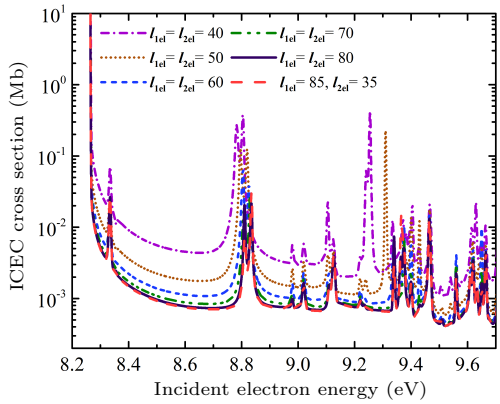


Fig. 3. ICEC cross section for H^+–Li with six different maximum values in the Legendre expansion of 1el and 2el for $R = 16$ Å.

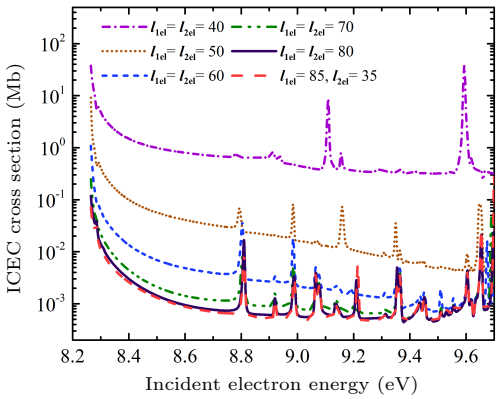


Fig. 4. ICEC cross section for H^+–He–Li with six different maximum values in the Legendre expansion of 1el and 2el for $R_1 = R_2 = 8$ Å.

Based on the preceding analysis, the optimal model for describing ICEC in the H^+–He–Li and H^+–Li systems combines the CAS(5,11) active space with the 6-311G(2df,2pd) basis set and employs maximum Legendre expansion orders of 85 for the one-electron integrals and 35 for the two-electron integrals. The results presented in the following section are based on this model.

4. Results and discussion

4.1. ICEC cross sections

Figure 5 presents the total cross sections, scaled by R^6, for three different internuclear distances R between H^+ and Li in the H^+–Li system. At $R = 4$ Å, the scaled cross section is on the order of 10^0. When R increases to 8 Å, the cross section decreases slightly. As the distance further increases from 8 Å to 16 Å, the cross section drops by approximately two orders of magnitude, reaching the order of 10^{-2} at $R = 16$ Å. It can be seen that as R increases, the ICEC cross section gradually decreases, mainly due to the reduction in orbital overlap between the atoms, which eventually leads to convergence toward the result of the virtual photon model. Our calculations are limited to $R \leq 16$ Å for two primary reasons. First, the computational cost increases significantly with larger internuclear distances. Second, accurately representing the continuum becomes increasingly difficult as the spatial extent of the system grows.

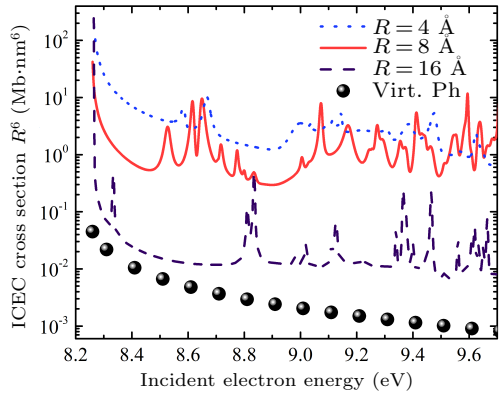


Fig. 5. ICEC cross sections for H^+–Li multiplied by R^6: *ab initio* results compared with the asymptotic one of Eq. (2).

The cross sections computed with the *R*-matrix approach can be compared with those obtained with the virtual photon approximation. It is valid in the limit of large *R* and provides an analytical formula for the cross sections:[2,3]

$$\sigma_{\mathrm{ICEC}}(\varepsilon) = \frac{3\hbar^4 c^2}{8\pi m_{\mathrm{e}}} \frac{g_{\mathrm{H}}}{g_{\mathrm{H}^+}} \frac{\sigma_{\mathrm{PI}}^{(\mathrm{H})}(\varepsilon)\,\sigma_{\mathrm{PI}}^{(\mathrm{Li})}(\varepsilon')}{\varepsilon R^6 E_{\mathrm{vph}}^2}. \tag{2}$$

While g_{H} and g_{H^+} are the statistical weights of the quantum states of H and H^+,[23] $\sigma_{\mathrm{PI}}^{(\mathrm{H})}(\varepsilon)$ and $\sigma_{\mathrm{PI}}^{(\mathrm{Li})}(\varepsilon')$ correspond to the photoionization cross sections of H at ε and Li at ε', respectively. E_{vph} represents the energy of the virtual photon, while *R* denotes the atomic separation distance. Several factors influence the efficiency of the ICEC process, including the energy of the incident electron (equivalent to the energy difference between the virtual photon and the ionization potential of the hydrogen atom), the photoionization cross sections of H and Li, and the distance between the interacting species. The ionization energy of He is notably high at 24.58 eV, rendering it incapable of participating in ICEC processes in the investigated region of energies. The ICEC cross sections for the H^+–He–Li system are not calculated using this formula. For the H^+–Li system, the electron affinity of the proton is 13.61 eV, and the ionization potential of Li is 5.39 eV, which ensures the ICEC channel remains open for all kinetic energies of the incident electron when the system is already in the initial H^+–Li state of the ICEC process. Additionally, the statistical weights are $g_{\mathrm{H}} = 2$, $g_{\mathrm{H}^+} = 1$. The photoionization cross sections used in this analysis were taken from Refs. [24,25].

The ICEC cross sections obtained using the virtual photon approximation for the H^+–Li system are presented in Fig. 5 for comparison. The cross section results from the *ab initio* calculations are at least two orders of magnitude higher than those predicted by the analytical formula at $R = 4$ Å and 8 Å. When the distance *R* increases to 16 Å, in the low-energy region, our calculations are close to the results of the virtual photon approximation. But at higher energies, our results are still higher. Molle *et al.*[7] investigated the ICEC cross section for the H^+–$\mathrm{H_2O}$ system and found that the *ab initio* ICEC cross sections below 6 Å are significantly larger than those predicted by the asymptotic formula. They attributed this substantial enhancement to orbital overlaps between H and $\mathrm{H_2O}$, which are neglected in the derivation of the asymptotic formula. In the present study for the H^+–Li system, the distance *R* between H^+ and Li ranges from 4 Å to 16 Å. The cross section results from *ab initio* calculations are higher than those from the analytical formula, indicating that orbital overlap between the proton and Li persists even at large separations.

Figure 6 shows the absolute cross sections of the ICEC of H^+–Li and H^+–He–Li at three different *R* with the values of 4 Å, 8 Å and 16 Å, respectively. For H^+–He–Li, when $R = 4$ Å, the ICEC cross section has the order of 10^2 Mb. When $R = 8$ Å, the ICEC cross section has the order of 10^0 Mb. With *R* increasing from 8 Å to 16 Å, the cross section decreases sharply by three orders and reaches the order of 10^{-3} Mb. Similarly, the H^+–Li system exhibits almost the same cross section magnitude. In general, the cross sections of the two systems exhibit the same trend with increasing *R*: they decrease. This is mainly due to the orbital overlap between atoms, which has been illustrated to enhance the *ab initio* ICEC cross section results between H and $\mathrm{H_2O}$.[7]

In order to study the intermediate He effect on the ICEC process, we compare the absolute cross sections of the ICEC of H^+–Li and H^+–He–Li. As shown in Fig. 6, both systems exhibit numerous resonance peaks. These peaks result from the temporary trapping of the emitted electron by the target system, leading to the formation of short-lived resonance states that manifest as peaks in the cross section. Notably, the cross section of the H^+–He–Li system exhibits more pronounced resonance features, which are particularly evident at $R = 16$ Å, as shown in the figure. This enhancement arises from the ability of the three-body system — unlike H^+–Li alone — to support additional H–He^-–Li^+ resonance states. These states significantly enhance the ICEC cross section, as clearly demonstrated in the figure. In the non-resonant energy region, however, the cross sections of H^+–Li and H^+–He–Li are comparable at $R = R = 4$ Å, 8 Å, and 16 Å, indicating that the presence of the He atom has minimal impact on the direct ICEC process between H^+ and Li.

Miteva *et al.*[10] demonstrated that, following inner-valence ionization of Ne in both NeHeNe and NeNe systems, the ICD process becomes six times faster in the presence of the bridging He atom. They attributed this enhancement to the intermediate virtual resonant states involving He^-. In our current study of the H^+–He–Li system, we observe more resonance peaks in the ICEC cross section compared with the H^+–Li case. While a detailed identification of all these resonances is challenging, we speculate that the additional peaks arise from resonant states such as H^+–He^-–Li or H–He^-–Li^+, indicating the formation of a He^--mediated virtual state. This observation is in good agreement with the conclusions of Miteva *et al*. Our results further demonstrate that when the ICEC process involves He^- as a virtual intermediate state, the cross section is significantly enhanced, reinforcing the notion that a third atom can facilitate energy transfer through virtual-state mediation. As discussed earlier, although ICD and ICEC are initiated by different processes, they share a common decay mechanism. The enhancement observed in both processes through the involvement of a third atom highlights a general strategy for controlling interatomic decay via virtual-state engineering.

Remme *et al.*[4] investigated both three-center resonant electron capture (rICEC) and direct (nonresonant) ICEC in the

H^+–He–Li system using an analytical approach. Their theoretical model shows that the cross section for three-center rICEC can be significantly enhanced compared to direct ICEC, in which the intermediate atom (He) does not participate. They reported a direct ICEC cross section of 2.2×10^{-23} cm^2 at $R_1 = R_2 = 5.3$ Å with an incident electron energy of 7.62 eV. In contrast, our calculations yield direct ICEC cross sections on the order of 10^{-19} cm^2 at $R = 10$ Å within the electron energy range of 8.26–9.76 eV, as shown in Fig. 6. Due to differences in methodology and the electron energy ranges considered, a direct quantitative comparison is not made. However, it is worth emphasizing that our approach accounts for orbital overlap, an effect neglected in the analytical model of Remme *et al*. Despite the quantitative differences, both studies lead to the same qualitative conclusion: the involvement of the helium atom in forming a virtual intermediate state can strongly enhance the ICEC cross section.

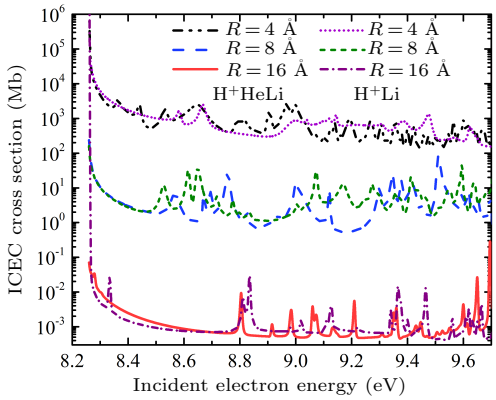


Fig. 6. A comparison of the absolute ICEC cross sections for H^+Li and H^+HeLi systems as functions of the incoming electron energy using the *R*-matrix approach.

4.2. ICEC resonance

A more detailed analysis of the energy dependence of the cross section can be carried out by examining the symmetry-resolved contributions. Figures 7 and 8 display the total and symmetry decomposition cross sections, based on 18-state CC calculations at $R = 16$ Å for the H^+–Li and H^+–He–Li systems. As illustrated in these figures, the $^1A_1$ and $^3A_1$ symmetries dominate the cross section. Our calculations reveal several resonance-like structures in the cross sections. These arise when an incoming electron temporarily forms a quasi-bound (resonant) state with the target, appearing as peaks in the cross section. In multichannel scattering, genuine resonances are identified not only by distinctive structures in the cross sections, but more definitively by a sharp π-radian jump in the eigenphase sum over a narrow energy interval. By analyzing the eigenphase sums obtained from the 18-state CC model, we determined the resonance parameters associated with three prominent sharp peaks. These values, along with tentative state assignments, are presented in Tables 2 and 3. All the observed states correspond to Feshbach resonances. All the resonance peaks in the ICEC cross section can, in principle, be identified by systematically removing different target states and varying the active space. However, in practice, many challenges arise that prevent the complete identification of all these peaks.

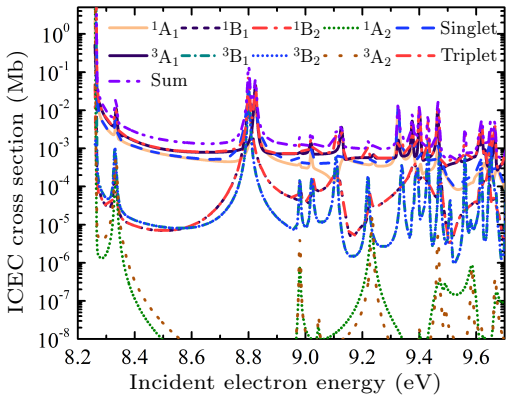


Fig. 7. Partial ICEC cross sections of H^+–Li obtained with the *R*-matrix approach for $R = 16$ Å.

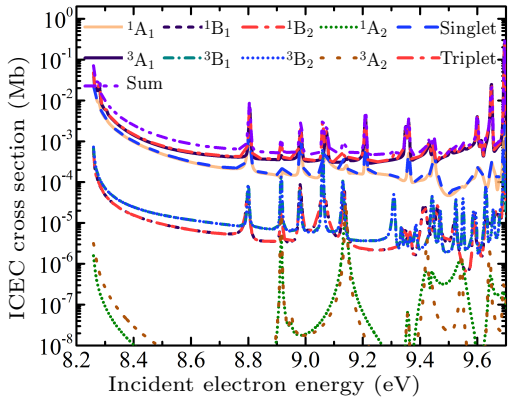


Fig. 8. Partial ICEC cross sections of H^+–He–Li obtained with the *R*-matrix approach for $R_1 = R_2 = 8$ Å.

Table 2. Resonant states of the e–H^+Li scattering system obtained with *R*-matrix approach for $R = 16$ Å.

	Resonance parameter		Parent state	
State	Position (eV)	Width (meV)	State	Position (eV)
$^1\Pi$ & $^3\Pi$	8.80	19 8.6	$1^2\Pi$	10.11
$^1\Sigma^+$ & $^3\Sigma^+$	8.82	7.5 7.8	$2^2\Sigma^+$	10.10
$^1\Sigma^+$ & $^3\Sigma^+$	9.02	7.9 10.3	$2^2\Sigma^+$	10.10
$^1\Pi$ & $^3\Pi$	9.02	9.1 9.2	$1^2\Pi$	10.11
$^1\Sigma^+$ & $^3\Sigma^+$	9.81	8.0 7.6	$4^2\Sigma^+$	12.82
$^1\Pi$ & $^3\Pi$	9.81	9.3 9.0	$2^2\Pi$	12.83

Table 3. Resonant states of the e–H^+HeLi scattering system obtained with *R*-matrix approach for $R_1 = R_2 = 8$ Å.

	Resonance parameter		Parent state	
State	Position (eV)	Width (meV)	State	Position (eV)
$^1\Sigma^+$ & $^3\Sigma^+$	8.80	10 7.9	$2^2\Sigma^+$	1.84
$^1\Pi$ & $^3\Pi$	8.80	6.9 6.5	$1^2\Pi$	1.85
$^1\Sigma^+$ & $^3\Sigma^+$	8.98	7.9 7.7	$2^2\Sigma^+$	1.84
$^1\Pi$ & $^3\Pi$	8.98	7.6 7.3	$1^2\Pi$	1.85
$^1\Sigma^+$ & $^3\Sigma^+$	9.69	8.5 6.0	$4^2\Sigma^+$	12.82
$^1\Pi$ & $^3\Pi$	9.69	7.7 7.6	$2^2\Pi$	12.83

As shown in Fig. 7, a pronounced double-peak structure appears in the cross section of the H^+–Li system near 8.81 eV, with the peaks located at 8.80 eV and 8.82 eV. The first peak corresponds to $^{1,3}\Pi$ symmetries with the electronic configuration $1\sigma^2 1\pi^2$, and it is associated with its parent state, $1^2\Pi$, via detachment of a 1π electron. The second peak is associated with $^{1,3}\Sigma^+$ symmetries, whose parent state is $2^2\Sigma^+$ with the configuration $1\sigma^2 2\sigma^2$ and $1\sigma^2 2\sigma 3\sigma$. A sharp peak is also observed at 9.02 eV in the $^{1,3}\Sigma^+$ cross sections. This feature arises from a resonance formed when a 3σ electron attaches to the $2^2\Sigma^+$ state, resulting in a configuration of $1\sigma^2 2\sigma 3\sigma$. This peak is also related to the $^{1,3}\Pi$ symmetries with a configuration of $1\sigma^2 1\pi 2\sigma$, which originate from the parent state $1^2\Pi$. At 9.81 eV, another set of peaks appears, involving both $^{1,3}\Sigma^+$ and $^{1,3}\Pi$ symmetries. The $^{1,3}\Sigma^+$ resonances have the parent state $4^2\Sigma^+$, while the $^{1,3}\Pi$ resonances originate from the $2^2\Pi$ state.

The same three resonance peaks also appear in the cross sections of the H^+–He–Li system, though slightly shifted in energy to 8.80 eV, 8.98 eV, and 9.69 eV, respectively, as shown in Fig. 8. These peaks exhibit the same resonance character as those in the H^+–Li system at 8.81 eV, 9.02 eV, and 9.81 eV. The small shifts in peak positions indicate that the inclusion of the He atom has only a minor effect on the original resonance states of the H^+–Li system. As shown in Fig. 6, the H^+–He–Li system exhibits a greater number of resonance peaks overall. This enhancement is attributed to the presence of the He atom, which alters the interaction dynamics and facilitates the formation of additional resonance states. Since multiple resonance peaks are present in these systems and the calculations involve complex interactions, it is difficult for us to identify which specific resonant states originate from the virtual states of He.

5. Conclusion

We have conducted a comprehensive study of the ICEC process in the H^+–Li and H^+–He–Li systems, reporting total cross sections, partial cross sections, and the resonance structure. The calculations were performed with the multichannel *R*-matrix method where a B-spline basis is employed to represent the continuum orbitals and the configuration interaction method is used to describe electronic correlation. This distinctive feature of the present calculations allowed us to generate an accurate description of the bound and continuum states.

We emphasize the convergence of the results and the accuracy of the target description for more complex systems: H^+–He–Li. In order to check such important effects as target polarization and the influence of coupling to the target continuum, we compared the results from three different active spaces with two different basis sets. We also checked the six combinations for the highest partial waves in the Legendre expansion for the one-electron and two-electron integrals. The differences between the results from these models provided an indication regarding the convergence of cross sections.

Using our most accurate model, we investigated the ICEC cross sections for the H^+–Li system to examine the role of an intermediate He atom in mediating energy transfer. The results show that the cross section is significantly enhanced when He^- is involved as a virtual intermediate state in the ICEC process. In contrast, when He does not participate in the mechanism, its presence has little effect on the direct ICEC process between H^+ and Li. This is evidenced by the comparable cross sections observed for the H^+–He–Li and H^+–Li systems.

We also compared the present results with other available studies. We find that introducing a He atom as an intermediate virtual resonant state can significantly enhance the Coulomb decay cross section. This finding is consistent with the results reported by Remme *et al.*[4] and Miteva *et al.*[10] However, our calculated direct ICEC cross sections are higher than those reported by Remme *et al.*,[4] which can be attributed to differences in the employed methodologies and the electron energy ranges considered.

The present calculations suggest that even atoms with no intrinsic ICEC activity can influence energy transfer when introduced into a system, thereby modulating the ICEC mechanism. This finding could facilitate experimental efforts aimed at measuring and validating ICEC processes. In realistic systems containing multiple adjacent atoms, the impact on ICEC may depend on the type, position, and number of bridging atoms. Although the presence of multiple bridge atoms may mimic the effect of several neighboring atoms on the ICEC cross section, the underlying mechanisms are likely more intricate and require further investigation.

Acknowledgements

This work was supported by the Natural Science Foundation of Henan Province (Grant No. 252300421490) and the Science Foundation of Henan Normal University (Grant No. 2021PL14). J.M. acknowledges support from the Natural Science Foundation of China (Grant No. 12304270).

References

[1] Bande A, Fasshauer E, Molle A, Peláez D, Pont F M and Sisourat N 2023 *J. Phys. B: At. Mol. Opt. Phys.* **56** 232001
[2] Gokhberg K and Cederbaum L S 2009 *J. Phys. B: At. Mol. Opt. Phys.* **42** 231001
[3] Gokhberg K and Cederbaum L S 2010 *Phys. Rev. A* **82** 052707
[4] Remme S, Voitkiv A B and Müller C 2023 *J. Phys. B: At. Mol. Opt. Phys.* **56** 095202
[5] Sisourat N, Miteva T, Gorfinkiel J D, Gokhberg K and Cederbaum L S 2018 *Phys. Rev. A* **98** 020701
[6] Molle A, Dubois A, Gorfinkiel J D, Cederbaum L S and Sisourat N 2021 *Phys. Rev. A* **103** 012808

[7] Molle A, Dubois A, Gorfinkiel J D, Cederbaum L S and Sisourat N 2021 *Phys. Rev. A.* **104** 022818

[8] Graves V, Šenk J, Kolorenč P, Sisourat N and Gorfinkiel J D 2024 *J. Chem. Phys.* **160** 204306

[9] Pont F M, Bande A, Fasshauer E, Molle A, Peláez D and Sisourat N 2024 *Phys. Rev. A* **110** 042804

[10] Miteva T, Kazandjian S, Kolorenč P, Votavová P and Sisourat N 2017 *Phys. Rev. Lett.* **119** 083403

[11] Bennett R, Votavová P, Kolorenč P, Miteva T, Sisourat N and Buhmann S Y 2019 *Phys. Rev. Lett.* **122** 153401

[12] Kuleff A I 2017 *Chem. Phys.* **482** 216

[13] Mullenix J B, Despré V and Kuleff A I 2020 *J. Phys. B: At. Mol. Opt. Phys.* **53** 184006

[14] Tennyson J 2010 *Phys. Rep.* **491** 29

[15] Su X, Cheng X, Cooper B, Tennyson J and Zhang H 2022 *Phys. Rev. A* **105** 062824

[16] Kaur S and Baluja K L 2005 *J. Phys. B: At. Mol. Opt. Phys.* **38** 3917

[17] Wang K, Zhang H, Huang X, Liu Y and Sun J 2018 *Phys. Rev. A* **97** 012703

[18] Burke P G 2011 *R-Matrix Theory of Atomic Collisions: Application to Atomic, Molecular and Optical Processes* (Springer-Verlag)

[19] Werner H J, Knowles P J, Knizia G, Manby F R, and Schütz M 2012 *WIREs Comput. Mol. Sci.* **2** 242

[20] Carr J M, Galiatsatos P G, Gorfinkiel J D, Harvey A G, Lysaght M A, Madden D, Mašín Z, Plummer M, Tennyson J and Varambhia H N 2012 *Eur. Phys. J. D* **66** 58

[21] Mašín Z, Benda J, Gorfinkiel J, Harvey A and Tennyson J 2019 *Comput. Phys. Commun.* **249** 107092

[22] Computational chemistry comparison and benchmark database

[23] Sobel'man I I 1972 *An Introduction to the Theory of Atomic Spectra* (Oxford: Pergamon)

[24] Leiden database for photodissociation and photoionization of astrophysically relevant molecules

[25] Heays A N, Bosman A D and Dishoeck E F van 2017 *Astron. Astrophys.* **602** A105